

Selective Denoising Diffusion Model for Time Series Anomaly Detection

Kohei Obata^{1*}, Zheng Chen¹, Yasuko Matsubara¹, Lingwei Zhu², Yasushi Sakurai¹

¹SANKEN, The University of Osaka, Osaka, Japan

²Great Bay University, Dongguan, China

{obata88, chenz, yasuko, yasushi}@sanken.osaka-u.ac.jp, zhulingwei@gbu.edu.cn

Abstract

Time series anomaly detection (TSAD) has been an important area of research for decades, with reconstruction-based methods, mostly based on generative models, gaining popularity and demonstrating success. Diffusion models have recently attracted attention due to their advanced generative capabilities. Existing diffusion-based methods for TSAD rely on a conditional strategy, which reconstructs input instances from white noise with the aid of the conditioner. However, this poses challenges in accurately reconstructing the normal parts, resulting in suboptimal detection performance. In response, we propose a novel diffusion-based method, named AnomalyFilter, which acts as a selective filter that only denoises anomaly parts in the instance while retaining normal parts. To build such a filter, we mask Gaussian noise during the training phase and conduct the denoising process without adding noise to the instances. The synergy of the two simple components greatly enhances the performance of naive diffusion models. Extensive experiments on five datasets demonstrate that AnomalyFilter achieves notably low reconstruction error on normal parts, providing empirical support for its effectiveness in anomaly detection. AnomalyFilter represents a pioneering approach that focuses on the noise design of diffusion models specifically tailored for TSAD.

Code — <https://github.com/KoheiObata/AnomalyFilter>

Introduction

Time series anomaly detection (TSAD) is an important task for real-world applications, including robot-assisted systems (Park, Hoshi, and Kemp 2018; Park et al. 2017), engines (Malhotra et al. 2016), and cyber-physical system maintenance (Tan, Ting, and Liu 2011). The goal of TSAD is to detect unexpected/unusual patterns/values within sequences that are significantly dissimilar to the majority. Since anomalies are typically rare and labeling them from quantities of data is laborious, TSAD is generally approached as an unsupervised learning problem in which detection relies on a normality assumption, namely, most observations are normal.

A prevalent approach for TSAD involves reconstruction-based methods. These methods learn to reconstruct normal samples during training and assume that normal sam-

ples are better reconstructed than anomalous samples during inference. Then, anomalies can be detected by thresholding the difference between the input and its reconstruction. Hence, the ideal reconstruction exhibits low reconstruction error on normal parts and high error on anomalous parts. Many methods, such as those based on GAN (Zhou et al. 2019; Bashar and Nayak 2020) and Transformer (Xu et al. 2022; Tuli, Casale, and Jennings 2022), are categorized as encoder-decoder models because they reconstruct samples from embeddings in latent space. However, controlling the balance between concise representation (i.e., regularization) and representation power (i.e., reconstruction) remains challenging (Gong et al. 2019). This issue is unavoidable when reconstructing from latent space.

Recently, diffusion models (Ho, Jain, and Abbeel 2020) have emerged as a promising approach due to their advanced generative capabilities (Zhang et al. 2023a). Unlike encoder-decoder models, diffusion models operate directly in data space, gradually reconstructing data from noisy inputs through an iterative denoising process. Current diffusion models for TSAD primarily focus on the creation of an effective conditional strategy of introducing inductive bias into the denoising process (Xiao et al. 2023; Chen et al. 2023). However, reconstructing from white noise proves challenging even with the aid of the conditioner due to the unavailability of original information. Consequently, while it denoises anomalous parts well and the reconstruction of anomalous parts deviates from the original input, it limits the accurate reconstruction of the normal parts.

Thus, a natural research question arises: *How can we accurately reconstruct the normal parts while exploiting the denoising capability of diffusion models?* In this work, we propose AnomalyFilter, a new diffusion-based method designed for TSAD, which overcomes the limitation of the existing diffusion-based methods regarding reconstruction quality. Specifically, we build a selective filter that denoises only the anomalous parts in the sample while retaining the normal parts. While alternative noise strategies for diffusion models have been explored in the image domain (Wyatt et al. 2022; Nachmani, Roman, and Wolf 2021), the impact of noise design on time series remains largely underexplored. Thus, we investigate the utility of *masked Gaussian noise*, which is the noise generated through a combination of Gaussian noise and Bernoulli mask. During the training, the

*Corresponding author.

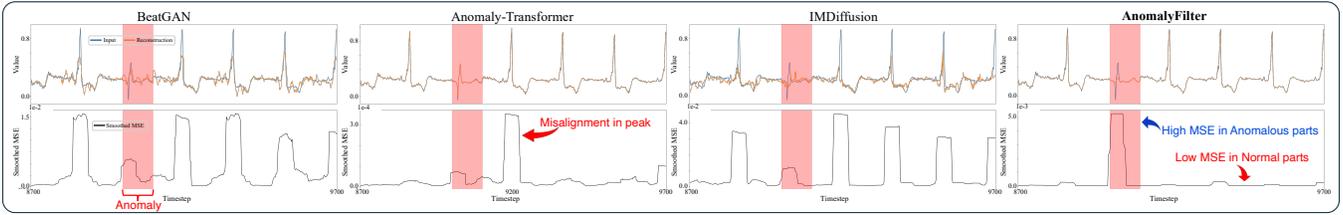


Figure 1: Reconstruction examples of encoder-decoder models (i.e., BeatGAN and Anomaly-Transformer), conditional diffusion models (i.e., IMDiffusion), and proposed AnomalyFilter.

model learn to predict the noise added to a sample similar to general diffusion models, enabling the model to act as a filter that selectively denoises nonmasked parts (i.e., erases Gaussian noise) while passing through masked parts (i.e., retains input). Furthermore, we observe that adding noise to the sample during the denoising process merely degrades reconstruction quality, leading to poor detection accuracy. To address this, we propose *noiseless inference*, which inputs a scaled noiseless sample into the model and conducts the denoising process without any noise, aligning seamlessly with the masked Gaussian noise. Neither masked Gaussian noise nor noiseless inference alone contributes significantly to improving the performance of the vanilla DDPM. However, the synergy of the two simple components allows the model to act as an effective filter, achieving substantial performance improvements over the vanilla DDPM.

Results Overview Figure 1 shows the reconstruction results and reconstruction error (i.e., MSE) of four methods. Remind that the y-axis units differ across methods. BeatGAN prioritizes concise expression and struggles at reconstructing peaks, resulting in consistently high MSE. Anomaly-Transformer, on the other hand, has strong representation power, causing it to accurately reconstruct even the anomalous parts, so-called “identical shortcut” issue (You et al. 2022). The relatively high MSE around 9200 is caused by a slight misalignment in reconstructing the peak. These results suggest that encoder-decoder models face challenges in balancing concise representation and representation power. IMDiffusion denoises anomalous parts well but fails to reconstruct normal parts, especially peaks, which demonstrates the limitation of conditional diffusion models. As a result, these methods fail to detect the anomalous parts. Our proposed AnomalyFilter shows a significantly higher MSE only in the anomalous parts while performing reconstruction with low MSE for the remaining parts, making anomaly detection easier.

Contributions In summary, this paper makes the following contributions:

- We investigate the limitations of the existing diffusion-based methods for TSAD from the perspective of noise design and empirically demonstrate their impact on reconstruction quality and anomaly detection performance.
- We introduce AnomalyFilter, a novel diffusion-based method designed for TSAD. It achieves ideal reconstruction, i.e., a low reconstruction error for normal parts and

relatively high reconstruction error for anomalous parts.

- We show the superiority of AnomalyFilter by comparing it with state-of-the-art baselines on five datasets. Notably, by combining two simple components, masked Gaussian noise and noiseless inference, we achieve a 45.1% improvement in VUS-PR compared with vanilla DDPM.

Related Work

Diffusion Model in Time Series Diffusion models are a type of generative model that gains the ability to generate diverse samples by corrupting training samples with noise and learning to reverse the process (Yang et al. 2023a; Lin et al. 2024). They have attracted increasing attention in the field of AI-generated content, such as text-to-image synthesis (Zhang et al. 2023a) and audio synthesis (Kong et al. 2021; Chen et al. 2021). As regards time series, conditional diffusion models have been applied to various time series tasks such as imputation (Wang et al. 2023; Zhang et al. 2023b; Fons et al. 2025) and forecasting (Alcaraz and Strodtzoff 2022; Feng et al. 2024; Li et al. 2024; Gao, Cao, and Chen 2025). They utilize diffusion models conditioned on observed values to impute/predict unseen values, achieving good success. For instance, CSDI (Tashiro et al. 2021) is designed for time series imputation, and it employs feature and temporal attention sequentially to learn the noise at each step while introducing conditions in the denoising process. TimeGrad (Rasul et al. 2021) is a conditional diffusion model that predicts in an autoregressive manner, with the denoising process guided by the hidden state of a recurrent neural network. Additionally, diffusion models have been employed for time series data augmentation (Huang, Chen, and Qiao 2024; Narasimhan et al. 2024; Kollovich et al. 2024; Li et al. 2025).

Diffusion Model for Time Series Anomaly Detection

TSAD differs from the aforementioned tasks in that all values are known. Overly powerful conditioners risk carrying anomaly information, which can lead to the accurate reconstruction of even anomalous parts. Therefore, the current mainstream focus is on a unique conditional strategy (Pintilie, Manolache, and Brad 2023; Wang et al. 2024a; Zhong et al. 2025). For example, IMDiffusion (Chen et al. 2023) is inspired by imputation techniques, where part of the sample is masked, and the unmasked parts serve as a condition to impute the masked parts. DiffAD (Xiao et al. 2023) tackles the case where anomalous points concentrate in certain parts, which is called anomaly concentration, and in-

incorporates a density ratio-based point selection strategy for masking anomalous parts. However, since they rely on partially observed input as a condition, which often loses information needed for reconstructing normal parts, their reconstruction errors are relatively high, resulting in a failure to detect anomalies that differ slightly from normalities (e.g., pattern-wise outliers).

Denoising Model for Anomaly Detection Denoising models, including diffusion models, perform anomaly detection by taking corrupted inputs, learning to denoise them, and generating clean reconstructions. Similar to diffusion models, a denoising autoencoder (DAE) (Vincent et al. 2010) adds noise (typically Gaussian) to the input but differs in that it directly predicts the clean input rather than using a stepwise denoising process. The selection of noise is critical in denoising models. Recent studies have explored deterministic noise (Bansal et al. 2024; Daras et al. 2022), and non-Gaussian noise (Nachmani, Roman, and Wolf 2021) for diffusion models. In image anomaly detection, (Kascenas et al. 2023) shows that DAE trained with coarse noise outperforms diffusion models at Brain MRI, and AnODDPM (Wyatt et al. 2022) demonstrates the effectiveness of Simplex noise. Despite these advancements in the image domain, where noise has been extensively studied and often operates on 2D data, noise tailored for time series remains largely unexplored. This highlights a significant gap in understanding the impact of noise design in TSAD applications.

Preliminaries

Problem Definition

In this paper, we focus on unsupervised anomaly detection for time series. We adopt a local contextual window to model their temporal dependency, which is a common practice with most deep TSAD methods. Consider an instance $\mathbf{X} = \{\mathbf{x}_1, \mathbf{x}_2, \dots, \mathbf{x}_L\} \in \mathbb{R}^{K \times L}$ to be a multivariate time series with K features and L timesteps. The objective of TSAD is to identify anomalous timesteps in a test set \mathcal{D}^{test} by training the model in an unlabeled training set \mathcal{D}^{train} assumed to contain mostly normal instances. Thus, the model aims to assign an anomaly score to each timestep, where higher scores are more anomalous. In a reconstruction-based approach, the model outputs a reconstruction $\hat{\mathbf{X}}$ of the given instance \mathbf{X} , and the anomaly score is calculated by comparing them by a score function $\mathcal{A}(\mathbf{x}_l, \hat{\mathbf{x}}_l) : \mathbb{R}^K \rightarrow \mathbb{R}$ (for simplicity, we consider the MSE score). To solve TSAD efficiently, we need a powerful method that achieves ideal reconstruction, i.e., has a low reconstruction error on the normal parts and a high reconstruction error on the anomalous parts of the instance.

Denoising Diffusion Probabilistic Model

Our AnomalyFilter is based on the denoising diffusion probabilistic model (DDPM) (Ho, Jain, and Abbeel 2020), a well-known diffusion model. DDPM consists of a forward diffusion process and a reverse denoising process. The forward diffusion process $q(\mathbf{X}_t | \mathbf{X}_{t-1})$ gradually corrupts data

Algorithm 1: Naive Training

- 1: **Input:** Training set \mathcal{D}^{train} , Forward diffusion step T ;
 - 2: **repeat**
 - 3: Sample data $\mathbf{X}_0 \sim \mathcal{D}^{train}$;
 - 4: Sample diffusion step $t \sim Uniform(\{1, \dots, T\})$;
 - 5: Sample noise $\epsilon_t \sim \mathcal{N}(\mathbf{0}, \mathbf{I})$;
 - 6: Corrupt $\mathbf{X}_t = \bar{\alpha}_t \mathbf{X}_0 + \sqrt{1 - \bar{\alpha}_t} \epsilon_t$;
 - 7: Calculate $\mathcal{L} = \|\epsilon_t - \epsilon_\theta(\mathbf{X}_t, t)\|$;
 - 8: **until** Converged;
-

from some target distribution $q(\mathbf{X}_0)$ into a normal distribution, where \mathbf{X}_t denotes corrupted data indexed by a diffusion step t . Thus, in practice, \mathbf{X}_0 is \mathbf{X} . Then, a learned reverse process $p_\theta(\mathbf{X}_{t-1} | \mathbf{X}_t)$ generates data by turning noise into data from $q(\mathbf{X}_0)$.

Forward Process This process can be formally described as Markovian:

$$q(\mathbf{X}_t | \mathbf{X}_{t-1}) = \mathcal{N}(\mathbf{X}_t; \sqrt{1 - \beta_t} \mathbf{X}_{t-1}, \beta_t \mathbf{I}), \quad (1)$$

for $t = \{1, \dots, T\}$, where T is a forward diffusion step. The variance schedule $\beta_t \in (0, 1)$ is a hyperparameter defined by a monotonically increasing sequence $\beta_1 < \beta_2 < \dots < \beta_T$ such that the data become sequentially corrupted.

To sample from an arbitrary t , namely without having to find intermediate steps $\mathbf{X}_{t-1}, \dots, \mathbf{X}_1$, the variance schedule is simplified to $\alpha_t = 1 - \beta_t$ and $\bar{\alpha}_t = \prod_{i=1}^t \alpha_i$, as follows:

$$q(\mathbf{X}_t | \mathbf{X}_0) = \mathcal{N}(\mathbf{X}_t; \sqrt{\bar{\alpha}_t} \mathbf{X}_0, (1 - \bar{\alpha}_t) \mathbf{I}), \quad (2)$$

$$\mathbf{X}_t = \bar{\alpha}_t \mathbf{X}_0 + \sqrt{1 - \bar{\alpha}_t} \epsilon_t, \quad (3)$$

where $\epsilon_t \sim \mathcal{N}(\mathbf{0}, \mathbf{I})$ is the same size as \mathbf{X}_0 .

Reverse Process The generative model, parameterized by θ , is a learned reverse process to denoise \mathbf{X}_T and reconstruct \mathbf{X}_0 . This is accomplished by iteratively computing the following Gaussian transitions:

$$p_\theta(\mathbf{X}_{t-1} | \mathbf{X}_t) = \mathcal{N}(\mathbf{X}_{t-1}; \mu_\theta(\mathbf{X}_t, t), \tilde{\beta}_t \mathbf{I}), \quad (4)$$

for $t = \{T, \dots, 1\}$, where $\tilde{\beta}_t = \frac{1 - \bar{\alpha}_{t-1}}{1 - \bar{\alpha}_t}$. μ_θ can, for example, be implemented with U-net-like architectures (Ronneberger, Fischer, and Brox 2015), and it can be learned by setting

$$\mu_\theta(\mathbf{X}_t, t) = \frac{1}{\alpha_t} \left(\mathbf{X}_t - \frac{\beta_t}{\sqrt{1 - \bar{\alpha}_t}} \epsilon_\theta(\mathbf{X}_t, t) \right). \quad (5)$$

Objective Function (Ho, Jain, and Abbeel 2020) shows that optimizing the following simplified training objective leads to better generation quality:

$$\mathcal{L} = \mathbb{E}_{\mathbf{X}_0 \sim q(\mathbf{X}_0), \epsilon_t \sim \mathcal{N}(\mathbf{0}, \mathbf{I}), t} [\|\epsilon_t - \epsilon_\theta(\mathbf{X}_t, t)\|], \quad (6)$$

where ϵ_t is the noise used to obtain \mathbf{X}_t from \mathbf{X}_0 in Equation (3) at step t , and $\|\cdot\|$ denotes the Frobenius norm.

Anomaly Detection with Diffusion Model

Here, we focus on general anomaly detection tasks that are not restricted to time series. The diffusion model is a reconstruction-based approach. Thus, hereafter, we describe the way in which the diffusion model reconstructs $\hat{\mathbf{X}}$.

Algorithm 2: Naive Inference

- 1: **Input:** Data $\mathbf{X}_0 \in \mathcal{D}^{test}$, Reverse diffusion step λ , Trained denoising function ϵ_θ ;
 - 2: **Output:** Reconstruction $\hat{\mathbf{X}}_0$ (i.e., $\hat{\mathbf{X}}$);
 - 3: Corrupt $\hat{\mathbf{X}}_\lambda = \bar{\alpha}_\lambda \mathbf{X}_0 + \sqrt{1 - \bar{\alpha}_\lambda} \epsilon_\lambda$;
 - 4: **for** $t = \lambda : 1$ **do**
 - 5: Sample $\epsilon_t \sim \mathcal{N}(\mathbf{0}, \mathbf{I})$ if $t > 1$ else $\epsilon_t = 0$;
 - 6: Denoise $\hat{\mathbf{X}}_{t-1} = \frac{1}{\sqrt{\alpha_t}} (\hat{\mathbf{X}}_t - \frac{\beta_t}{\sqrt{1 - \bar{\alpha}_t}} \epsilon_\theta(\hat{\mathbf{X}}_t, t)) + \tilde{\beta}_t \epsilon_t$;
 - 7: **end for**
 - 8: **return** $\hat{\mathbf{X}}_0$;
-

Training Phase During the training phase, the model ϵ_θ learns to predict the noise ϵ_t added to $\mathbf{X}_0 \in \mathcal{D}^{train}$ given \mathbf{X}_t and t . The training procedure is shown as Algorithm 1. In each iteration of the training (Line 3-7), a diffusion step t is randomly sampled, at which point the diffusion process Equation (3) is applied. Unlike the other tasks, in anomaly detection, \mathbf{X}_T does not need to be white noise. The loss Equation (6) is calculated afterward.

Inference Phase In the inference phase, the model ϵ_θ generates a reconstruction $\hat{\mathbf{X}}$ given the input instance $\mathbf{X}_0 \in \mathcal{D}^{test}$. The inference procedure is shown in Algorithm 2. It first corrupts \mathbf{X}_0 into $\hat{\mathbf{X}}_\lambda$ (Line 3):

$$\hat{\mathbf{X}}_\lambda = \bar{\alpha}_\lambda \mathbf{X}_0 + \sqrt{1 - \bar{\alpha}_\lambda} \epsilon_\lambda, \quad (7)$$

where λ is a reverse diffusion step that can be shorter than T . In general, relatively weak noise is added to form $\hat{\mathbf{X}}_\lambda$ so that it retains some of the input features (Wyatt et al. 2022; Pintilie, Manolache, and Brad 2023). This can be seen as a conditional DDPM on the input instance. Then, in each step (Line 6), $\hat{\mathbf{X}}_\lambda$ is gradually denoised to reconstruct $\hat{\mathbf{X}}$.

$$\hat{\mathbf{X}}_{t-1} = \frac{1}{\sqrt{\alpha_t}} (\hat{\mathbf{X}}_t - \frac{\beta_t}{\sqrt{1 - \bar{\alpha}_t}} \epsilon_\theta(\hat{\mathbf{X}}_t, t)) + \tilde{\beta}_t \epsilon_t. \quad (8)$$

Proposed AnomalyFilter

In this section, we propose AnomalyFilter, a novel diffusion-based method designed for TSAD, which works as a selective filter that removes only the anomalous parts while retaining the normal parts. We begin by providing an overview of AnomalyFilter and its architecture. Subsequently, we look at how to achieve such a filter.

Overview An overview of the AnomalyFilter framework is in Figure 2 (left). It consists of *masked Gaussian noise training* and *noiseless inference*. Masked Gaussian noise makes the model learn to allow normal parts to pass through selectively by masking the Gaussian noise. To address the reconstruction quality issue, we propose noiseless inference, which eliminates the addition of noise during the inference. This aligns with the learned masked Gaussian noise and achieves the accurate reconstruction of normal parts.

Architecture The architecture of AnomalyFilter is shown in Figure 2 (right) and is based on CSDI (Tashiro et al. 2021), which is a modification of DiffWave (Kong et al.

Algorithm 3: Masked Gaussian Noise Training

- 1: **Input:** Training set \mathcal{D}^{train} , Forward diffusion step T , Mask ratio p ;
 - 2: **repeat**
 - 3: Sample data $\mathbf{X}_0 \sim \mathcal{D}^{train}$;
 - 4: Sample diffusion step $t \sim Uniform(\{1, \dots, T\})$;
 - 5: Sample noise $\epsilon_t = \mathbf{B} \circ \zeta$, where $\zeta \sim \mathcal{N}(\mathbf{0}, \mathbf{I})$, $\mathbf{B}_{k,l} \sim Bernoulli(p)$;
 - 6: Corrupt $\mathbf{X}_t = \bar{\alpha}_t \mathbf{X}_0 + \sqrt{1 - \bar{\alpha}_t} \epsilon_t$;
 - 7: Calculate $\mathcal{L} = \|\epsilon_t - \epsilon_\theta(\mathbf{X}_t, t)\|$;
 - 8: **until** Converged;
-

2021) employing transformer layers. It is composed of multiple residual layers with a latent dimension C . Diffusion step t is embedded as a 128-dimensional encoding vector with positional encoding (Vaswani et al. 2017) and input into the model together with data \mathbf{X}_t . To incorporate temporal and inter-variable dependencies beyond L timesteps and K features, we employ a temporal and feature transformer layer. The positional encoding of time and feature is added afterward. As is typical for diffusion models, the output dimensions match the input dimensions.

Masked Gaussian Noise

Our objective is to build a filter with two functionalities: (1) removing the anomalous parts and (2) allowing the normal parts to pass through. We design masked Gaussian noise for this purpose. Specifically, we represent anomalous parts with Gaussian noise, as in typical DDPM. To enable the model to allow normal parts to pass through, we randomly mask the noise. The stochastic selection of the noise to mask enables the filter to selectively denoise anomalous parts. Formally, our masked Gaussian noise ϵ_t is defined as follows:

$$\epsilon_t = \mathbf{B} \circ \zeta, \quad (9)$$

where \circ is element-wise multiplication, $\zeta \sim \mathcal{N}(\mathbf{0}, \mathbf{I})$ is Gaussian noise, and \mathbf{B} is a mask with elements drawn from a Bernoulli distribution, $\mathbf{B}_{k,l} \sim Bernoulli(p)$. The hyperparameter p controls the mask ratio; the larger the value, the larger the ratio of Gaussian noise.

Masked Gaussian Noise Training

The simplified DDPM loss function Equation (6) can be interpreted as training the model to predict the noise added to the data. Similarly, we train our model ϵ_θ to predict the masked Gaussian noise ϵ_t .

Algorithm The training procedure for AnomalyFilter is summarized in Algorithm 3, where the differences from the conventional algorithm (Algorithm 1) are highlighted in cyan. We follow the conventional training procedure for the diffusion model except for the noise ϵ_t (Line 5). Specifically, given data \mathbf{X}_0 , we sample noisy data \mathbf{X}_t and train ϵ_θ by minimizing the loss function in Equation (6).

Objective Function Although we use a loss function similar to that of DDPM, with the introduction of masked Gaus-

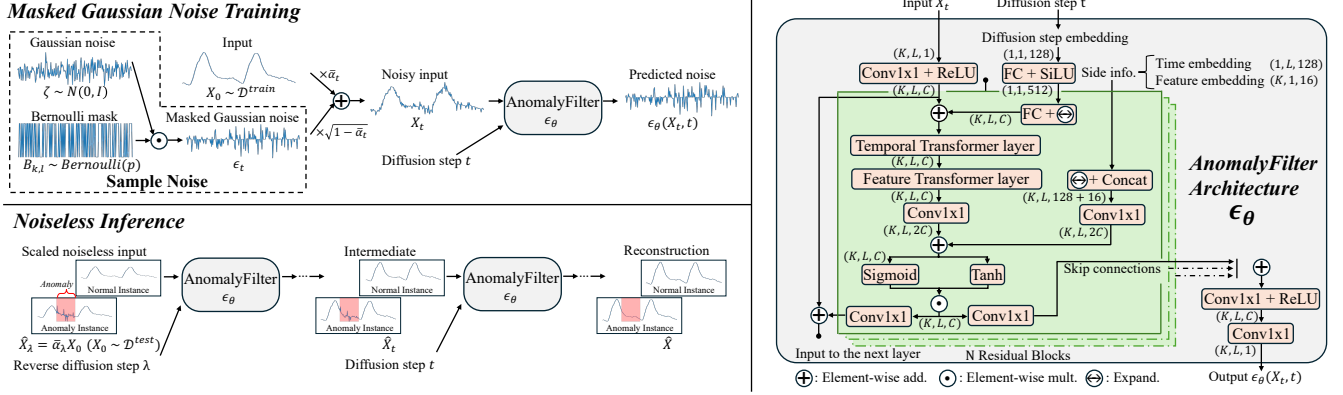


Figure 2: An overview of AnomalyFilter framework. The model is trained to predict masked Gaussian noise, with the aim of learning to denoise the anomaly parts (i.e., nonmasked parts) and retaining the normal parts (i.e., masked parts). Noiseless inference operates without noise at the beginning and during the denoising steps. Thus, when given a normal instance, it outputs an instance with no change. When given an anomaly instance, only anomalous parts are removed. AnomalyFilter captures temporal and inter-variable dependencies by temporal and feature transformer layers and predicts noise added to the input.

Algorithm 4: Noiseless Inference

- 1: **Input:** Data $\mathbf{X}_0 \in \mathcal{D}^{test}$, Reverse diffusion step λ , Trained denoising function ϵ_θ ;
 - 2: **Output:** Reconstruction $\hat{\mathbf{X}}_0$ (i.e., $\hat{\mathbf{X}}$);
 - 3: **Scale** $\hat{\mathbf{X}}_\lambda = \bar{\alpha}_\lambda \mathbf{X}_0$;
 - 4: **for** $t = \lambda : 1$ **do**
 - 5: **Denoise** $\hat{\mathbf{X}}_{t-1} = \frac{1}{\sqrt{\alpha_t}} (\hat{\mathbf{X}}_t - \frac{\beta_t}{\sqrt{1-\alpha_t}} \epsilon_\theta(\hat{\mathbf{X}}_t, t))$;
 - 6: **end for**
 - 7: **return** $\hat{\mathbf{X}}_0$;
-

sian noise, our loss function can be divided into two parts.

$$\begin{aligned}
 \mathcal{L} &= \mathbb{E}[\|\epsilon_t - \epsilon_\theta(\mathbf{X}_t, t)\|] \\
 &= \underbrace{\mathbb{E}[\mathbf{B} \circ \|\zeta - \epsilon_\theta(\mathbf{X}_t, t)\|]}_{\text{Noiseless part}} + \underbrace{\mathbb{E}[(\mathbf{1} - \mathbf{B}) \circ \|\mathbf{0} - \epsilon_\theta(\mathbf{X}_t, t)\|]}_{\text{Noise part}} \\
 &= \mathcal{L}_{NonMask} + \mathcal{L}_{Mask}.
 \end{aligned} \tag{10}$$

The derivation is provided in the Appendix. Thus, this loss function enables the model to learn a filter with two functionalities: (1) the removal of anomalous parts ($\mathcal{L}_{NonMask}$) and (2) the retention of normal parts (\mathcal{L}_{Mask}).

Noiseless Inference

To achieve low reconstruction errors for normal parts, we introduce noiseless inference, which inputs the data as they are and does not add noise at each denoising step. Algorithm 4 is our proposed noiseless inference. Instead of inputting corrupted data $\hat{\mathbf{X}}_\lambda = \bar{\alpha}_\lambda \mathbf{X}_0 + \sqrt{1 - \bar{\alpha}_\lambda} \epsilon_\lambda$ into the model, we input the following scaled noiseless data (Line 3):

$$\hat{\mathbf{X}}_\lambda = \bar{\alpha}_\lambda \mathbf{X}_0. \tag{11}$$

Then, at each denoising step, \mathbf{X}_λ is gradually denoised to reconstruct $\hat{\mathbf{X}}$. This step is conducted without any addition

of noise (Line 5):

$$\hat{\mathbf{X}}_{t-1} = \frac{1}{\sqrt{\alpha_t}} (\hat{\mathbf{X}}_t - \frac{\beta_t}{\sqrt{1-\alpha_t}} \epsilon_\theta(\hat{\mathbf{X}}_t, t)). \tag{12}$$

Thanks to the masked Gaussian noise, the model functions as a filter. Thus, noiseless inference presumes that the model outputs data with no change when given normal data and outputs data with the anomalous parts removed when given anomaly data. The key advantage of noiseless inference over naive inference (Algorithm 2) is that it prevents the loss of important features of the original input, which occurs by adding noise. This allows the input to act as a condition for reconstruction, leading to an accurate reconstruction of the normal parts.

Experiments

Experiment Setup

Datasets We use five datasets in our paper: (1) UCR anomaly archive (UCR) (Wu and Keogh 2021), (2) AIOps, (3, 4) Yahoo real and Yahoo bench, and (5) Server Machine Dataset (SMD) (Su et al. 2019). We trained and tested separately for each of the subdatasets, and the average results of five runs are presented.

Baselines We compare our method with the following 13 baselines in four categories, including classical methods and state-of-the-art reconstruction-based methods, as follows: (1) Classical machine-learning methods, IsolationForest (Liu, Ting, and Zhou 2008) and OCSVM (Schölkopf et al. 1999), (2) GAN, VAE, and AE-based methods, BeatGAN (Zhou et al. 2019), LSTM-VAE (Park, Hoshi, and Kemp 2018), and USAD (Audibert et al. 2020), (3) Transformer-based methods, Anomaly-Transformer (Xu et al. 2022), TranAD (Tuli, Casale, and Jennings 2022), and DADA (Shentu et al. 2025), and (4) Denoising-based methods, DiffAD (Xiao et al. 2023), IMDiffusion (Chen et al.

	UCR				AIOps			Yahoo real			Yahoo bench			SMD		
	V-R	V-P	RF	Acc.	V-R	V-P	RF									
IsolationForest	0.641	0.106	0.041	0.236	0.798	0.169	0.061	0.699	0.358	0.000	0.611	0.295	0.000	0.735	0.245	0.093
OCSVM	0.645	0.167	0.092	0.300	0.848	0.336	0.152	0.715	0.443	0.000	0.608	0.289	0.000	0.698	0.239	0.156
BeatGAN	0.746	<u>0.205</u>	<u>0.137</u>	<u>0.351</u>	<u>0.889</u>	<u>0.487</u>	0.239	0.751	0.503	0.060	0.720	<u>0.373</u>	0.004	0.819	0.356	0.232
LSTM-VAE	<u>0.739</u>	0.141	0.113	0.217	0.864	0.359	0.185	<u>0.899</u>	<u>0.612</u>	0.076	0.709	0.329	0.003	0.711	0.223	0.190
USAD	0.674	0.156	0.129	0.272	<u>0.889</u>	0.445	0.227	0.830	0.571	0.075	0.612	0.305	0.000	0.508	0.145	0.088
Anomaly-Transformer	0.704	0.132	0.103	0.202	0.881	0.347	0.157	0.872	0.557	0.051	0.710	0.291	0.005	0.861	<u>0.420</u>	0.252
TranAD	0.579	0.072	0.059	0.157	0.762	0.230	0.160	0.774	0.496	0.061	0.589	0.270	0.000	0.636	0.194	0.144
DADA	0.585	0.028	0.015	0.036	0.839	0.255	0.161	0.860	0.548	0.095	0.745	0.309	<u>0.007</u>	<u>0.875</u>	0.419	<u>0.262</u>
DiffAD	0.605	0.063	0.039	0.095	0.859	0.395	0.191	0.844	0.520	0.077	<u>0.768</u>	0.346	0.004	0.606	0.169	0.157
IMDiffusion	0.630	0.047	0.028	0.060	0.866	0.358	0.126	0.860	0.552	0.062	0.725	0.300	0.002	0.850	0.341	0.196
D3R	0.580	0.071	0.060	0.157	0.839	0.396	0.213	0.839	0.560	<u>0.099</u>	0.668	0.315	0.000	0.828	0.330	0.235
AnomalyFilter	0.726	0.238	0.204	0.399	0.932	0.597	<u>0.230</u>	0.900	0.625	0.109	0.793	0.416	0.011	0.891	0.477	0.273

Table 1: Anomaly detection performance. V-R and V-P are VUS-ROC and VUS-PR (Paparrizos et al. 2022). RF is Range F-score (Tatbul et al. 2018). Best results are in **bold**, and second-best results are underlined (higher is better).

	UCR				AIOps			Yahoo real			Yahoo bench			SMD		
	V-R	V-P	RF	Acc	V-R	V-P	RF									
DAE	0.760	0.252	<u>0.190</u>	<u>0.386</u>	0.900	0.501	0.266	0.888	0.614	<u>0.083</u>	0.694	0.310	0.003	0.866	0.435	0.238
DAE w/ M	0.685	0.149	0.125	0.266	0.890	0.495	0.243	0.894	0.606	0.080	0.688	0.286	0.001	<u>0.878</u>	0.452	0.257
DAE w/ N	<u>0.758</u>	0.234	0.173	0.382	0.884	0.448	<u>0.257</u>	0.887	0.593	0.073	0.687	0.284	0.001	0.875	<u>0.456</u>	0.255
DAE w/ M&N	0.693	0.172	0.144	0.291	<u>0.915</u>	<u>0.519</u>	0.242	0.905	<u>0.624</u>	0.081	0.696	<u>0.316</u>	<u>0.004</u>	0.876	0.439	0.265
DDPM	0.660	0.071	0.054	0.110	0.761	0.183	0.100	0.865	0.550	0.064	0.714	0.280	0.001	0.786	0.337	<u>0.267</u>
DDPM w/ M	0.660	0.062	0.046	0.097	0.713	0.162	0.079	0.843	0.508	0.074	0.717	0.268	0.000	0.751	0.286	0.228
DDPM w/ N	0.709	0.165	0.127	0.272	0.827	0.323	0.204	0.896	0.613	<u>0.083</u>	<u>0.727</u>	0.313	0.000	0.812	0.334	0.233
AnomalyFilter (DDPM w/ M&N)	0.726	<u>0.238</u>	0.204	0.399	0.932	0.597	0.230	<u>0.900</u>	0.625	0.109	0.793	0.416	0.011	0.891	0.477	0.273

Table 2: Ablation study with different components. M and N refer to Bernoulli mask and Noiseless inference, respectively.

2023), D3R (Wang et al. 2024b), DAE (Vincent et al. 2010) and DDPM (Ho, Jain, and Abbeel 2020). We position DAE and DDPM as part of our ablation study, since they share the same architecture as AnomalyFilter.

Evaluation Metrics It is claimed that the traditional metric for TSAD, namely the F1 score calculated with a protocol named point adjustment (PA), overestimates the model performance (Kim et al. 2022; Sarfraz et al. 2024). Thus, we adopt various threshold-independent measures along with conventional metrics (AUC-ROC and F1 score) for a comprehensive comparison. Specifically, we use the following five range-based measures, which are designed to provide a robust and suitable assessment for TSAD. Range F-score (Tatbul et al. 2018), Range-AUC-ROC, Range-AUC-PR, volume under the surface (VUS)-ROC, and VUS-PR (Paparrizos et al. 2022). In particular, VUS-PR is identified as providing the most reliable and accurate measurement (Liu and Paparrizos 2024). We set the buffer region for Range-AUC-ROC/PR at half of the window size. For UCR, we also employ accuracy as a metric, where we consider that the model detects the anomaly if the highest anomaly score is located inside the given anomaly range, since it only has a single anomaly in a sequence.

Anomaly Detection Performance

Table 1 presents the performance of AnomalyFilter and the baseline methods for five datasets. While the second-best method varies depending on the dataset and metric, the proposed AnomalyFilter achieves the highest detection accuracy across most of the datasets, demonstrating an average improvement of 4.1% in VOC-ROC, 14.4% in VOC-PR,

and 29.0% in Range F-score compared with the second-best method. Overall, reconstruction-based methods exceed classic machine-learning methods. BeatGAN struggles with Yahoo, which has limited training data, and SMD, which is multivariate data. In contrast, Anomaly-Transformer performs well on SMD, but tends to overfit on simple patterns, as shown in Figure 1, and underperforms on UCR. These results highlight the difficulty of appropriately balancing the information bottleneck across diverse datasets. DADA is a zero-shot anomaly detection method that identifies relative anomalies within a window. However, when most values in a window are anomalous (as in UCR), it fails to detect them accurately, resulting in lower performance. Diffusion-based methods, DiffAD and IMDiffusion, face challenges in UCR, which contains many pattern-wise anomalies, reflecting limitations in the reconstruction quality. These results demonstrate the effectiveness of AnomalyFilter.

Ablation Studies

We assess the contribution of each component. Qualitative analysis, hyperparameter studies, and case studies can be found in the Appendix.

Effect of key components Table 2 shows quantitative results across datasets w/o each component with DAE and DDPM as a base method. We can see that the noiseless inference enhances the performance of the vanilla DDPM. While the Bernoulli mask alone does not independently improve the accuracy of DDPM, its combination with noiseless, namely AnomalyFilter, leads to substantial performance gains. This synergy underscores the importance of jointly employing these two simple components in improv-

	UCR			AIOps			Yahoo real			Yahoo bench			SMD		
	MSE_a	MSE_n	$\frac{MSE_a}{MSE_n}$	MSE_a	MSE_n	$\frac{MSE_a}{MSE_n}$	MSE_a	MSE_n	$\frac{MSE_a}{MSE_n}$	MSE_a	MSE_n	$\frac{MSE_a}{MSE_n}$	MSE_a	MSE_n	$\frac{MSE_a}{MSE_n}$
BeatGAN	0.0153	0.0030	5.1	0.0251	0.0005	50.6	9.6410	0.3539	27.2	0.0660	0.0296	2.2	0.0257	0.0053	4.8
LSTM-VAE	0.0171	0.0030	5.7	0.0361	0.0014	25.5	10.6639	0.3497	30.5	<u>0.1656</u>	0.1131	1.5	<u>0.0387</u>	0.0130	3.0
USAD	0.0394	0.0152	2.6	<u>0.0715</u>	0.0068	10.5	<u>12.6297</u>	0.7915	16.0	0.1593	0.1265	1.3	0.0036	0.0015	2.3
Anomaly-Transformer	0.0039	0.0004	<u>10.3</u>	0.0091	<u>0.0002</u>	50.7	9.6449	0.2966	32.5	0.0266	0.0133	2.0	0.0239	0.0042	5.6
TranAD	0.0447	0.0328	1.4	0.0892	0.0187	4.8	12.6501	0.8379	15.1	0.2679	0.2464	1.1	0.0183	0.0032	5.8
DADA	0.0090	0.0050	1.8	0.0072	0.0003	23.0	2.2592	<u>0.0204</u>	110.8	0.0195	0.0059	3.3	0.0029	0.0006	4.8
DiffAD	0.0373	0.0244	1.5	0.0436	0.0051	8.5	10.4784	0.2780	37.70	0.0844	0.0362	2.3	0.0490	0.0314	1.6
IMDiffusion	<u>0.0532</u>	0.0273	1.9	0.0501	0.0110	4.6	10.0372	0.2937	34.2	0.1038	0.0528	2.0	0.0150	0.0031	4.8
D3R	0.0540	0.0440	1.2	0.0476	0.0094	5.0	10.0916	0.1463	<u>69.0</u>	0.0636	0.0252	2.5	0.0142	0.0028	5.0
AnomalyFilter	0.0108	<u>0.0008</u>	13.9	0.0344	0.0001	257.3	0.3551	0.0075	47.2	0.0276	<u>0.0070</u>	4.0	0.0093	<u>0.0010</u>	9.5
DAE	0.0103	0.0016	6.7	0.0374	0.0006	<u>66.7</u>	10.3125	0.3423	30.1	0.0642	0.0382	1.7	0.0037	0.0006	<u>6.0</u>
DDPM	0.0357	0.0170	2.1	0.0415	0.0053	7.8	0.5271	0.0716	7.4	0.0917	0.0472	1.9	0.0155	0.0053	3.0
DDPM w/ N	0.0261	0.0080	3.3	0.0392	0.0026	15.1	0.4989	0.0401	12.4	0.0757	0.0311	2.4	0.0139	0.0046	3.0
DDPM w/ M	0.0339	0.0201	1.7	0.0472	0.0111	4.3	0.4564	0.0690	6.6	0.0837	0.0511	1.6	0.0250	0.0169	1.5

Table 3: Reconstruction quality performance. MSE_a and MSE_n are the MSE values of anomalous and normal parts during the inference. Not necessary, but MSE_a should be higher, and MSE_n should be lower. The higher the ratio $\frac{MSE_a}{MSE_n}$ is, the easier it is to detect anomalies.

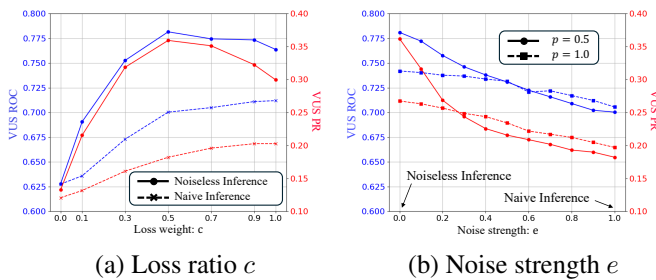


Figure 3: Effect of loss weights and noise strength.

ing anomaly detection capabilities. The failure of the mask to work effectively on its own is because, in naive inference, noise is added at each denoising step, resulting in a mismatch with what the model has learned. Interestingly, when DAE is used as the base method, neither the Bernoulli mask nor noiseless inference contributes to performance improvement. This is probably because the direct prediction framework of DAE makes it challenging to learn a complex filter capable of both retaining and denoising, while DDPM has demonstrated remarkable capabilities in learning the filter.

Effect of loss weights We investigate the effect of loss weights. During our experiments, we give the same importance to each regularizer, i.e., the coefficients c in $\mathcal{L} = c\mathcal{L}_{NonMask} + (1 - c)\mathcal{L}_{Mask}$ are set at 0.5. Here, we vary c from $\{0.1, \dots, 1.0\}$, using $p = 0.5$ for training, where $c = 1.0$ focused solely on denoising and $c = 0.0$ focused solely on retention. The results, shown in Figure 3 (a), indicate that $c = 0.5$ achieved the best performance, aligning with $p = 0.5$ and suggesting that explicit weighting is unnecessary. However, under naive inference, $c = 1.0$ performed best, demonstrating that denoising is critical when inference includes noise, whereas both processes are significant when inference is noise-free.

Effect of noise strength during inference We evaluate the effect of noiseless inference by modifying the noise added during naive inference (Algorithm 2, Lines 3 and 6) from ϵ_t to $e\epsilon_t$ and gradually reducing e from $\{1.0, \dots, 0.0\}$,

even achieving noiseless inference. This is equivalent to sampling Gaussian noise ζ from $\mathcal{N}(\mathbf{0}, e^2\mathbf{I})$. Figure 3 (b) shows the results for models trained with masked Gaussian noise ($p = 0.5$) and Gaussian noise ($p = 1.0$). In both cases, the performance improved as e decreased, with the best results achieved at $e = 0.0$ (i.e., noiseless inference), indicating that noise is unnecessary for inference in TSAD. The model trained on Gaussian noise outperformed masked Gaussian noise at around $e \geq 0.4$, suggesting that models trained with Gaussian noise are more suitable when inference includes higher levels of noise, aligning with their training paradigm.

Reconstruction Quality

We show the MSE of anomalous and normal parts and their ratio in Table 3. Compared to baselines and ablation settings, AnomalyFilter achieves a significantly lower MSE_n , resulting in a larger ratio $\frac{MSE_a}{MSE_n}$. This demonstrates that AnomalyFilter is well-suited for effective anomaly detection. Although Anomaly-Transformer achieves a very small MSE_n on UCR and AIOps, its MSE_a is similarly small, resulting in a mediocre ratio. As illustrated in Figure 1, this causes false positives by even slight misalignments in normal regions. DADA, a zero-shot anomaly detector, shows favorable ratios on datasets like Yahoo, where the number of training samples is limited and point anomalies are dominant, but struggles in UCR, which contains longer anomalous parts than the window size. Diffusion-based methods such as DiffAD, IMDiffusion, and DDPM exhibit high values in both MSE_a and MSE_n , indicating the limitation of diffusion models. DDPM w/ Mask yields results similar to the vanilla DDPM, suggesting that the Bernoulli mask by itself is not sufficient for improving detection ability. In contrast, DDPM w/ Noiseless setting shows a notable reduction in MSE_n , leading to improved ratio. These findings are consistent with the anomaly detection performance reported in Table 2 and further support the effectiveness of the proposed approach, particularly the combined contribution of the Bernoulli mask and noiseless inference.

Conclusion

We proposed a novel diffusion-based method called AnomalyFilter for unsupervised TSAD. To resolve the low reconstruction quality of existing reconstruction-based methods, we built a selective filter that accurately denoises anomalous parts while retaining normal parts. Specifically, we investigated the utility of noise in diffusion models and devised masked Gaussian noise and noiseless inference. Extensive experiments on five datasets demonstrated the effectiveness of the method. Ablation studies confirmed the contribution of our design to anomaly detection in a quantitative and qualitative manner and demonstrated that the synergy of the proposed two simple components strongly enhances vanilla DDPM. Overall, we believe that our work paves the way for a new diffusion-based approach towards TSAD.

Acknowledgments

The authors would like to thank the anonymous referees for their valuable comments and helpful suggestions. This work was supported by JST CREST JPMJCR23M3, JST START JPMJST2553, JST CREST JPMJCR20C6, JST K Program JPMJKP25Y6, JST COI-NEXT JPMJPF2009, JST COI-NEXT JPMJPF2115, the Future Social Value Co-Creation Project - Osaka University.

References

- Alcaraz, J. L.; and Strodthoff, N. 2022. Diffusion-based Time Series Imputation and Forecasting with Structured State Space Models. *TMLR*.
- Audibert, J.; Michiardi, P.; Guyard, F.; Marti, S.; and Zuluaga, M. A. 2020. Usad: Unsupervised anomaly detection on multivariate time series. In *KDD*, 3395–3404.
- Bansal, A.; Borgnia, E.; Chu, H.-M.; Li, J.; Kazemi, H.; Huang, F.; Goldblum, M.; Geiping, J.; and Goldstein, T. 2024. Cold diffusion: Inverting arbitrary image transforms without noise. *NeurIPS*, 36.
- Bashar, M. A.; and Nayak, R. 2020. TAnoGAN: Time series anomaly detection with generative adversarial networks. In *2020 IEEE Symposium Series on Computational Intelligence (SSCI)*, 1778–1785. IEEE.
- Challu, C. I.; Jiang, P.; Wu, Y. N.; and Callot, L. 2022. Deep generative model with hierarchical latent factors for time series anomaly detection. In *AISTATS*, 1643–1654. PMLR.
- Chen, N.; Zhang, Y.; Zen, H.; Weiss, R. J.; Norouzi, M.; and Chan, W. 2021. WaveGrad: Estimating Gradients for Waveform Generation. In *ICLR*.
- Chen, Y.; Zhang, C.; Ma, M.; Liu, Y.; Ding, R.; Li, B.; He, S.; Rajmohan, S.; Lin, Q.; and Zhang, D. 2023. ImDiffusion: Imputed Diffusion Models for Multivariate Time Series Anomaly Detection. *Proc. VLDB Endow.*, 17(3): 359–372.
- Daras, G.; Delbraccio, M.; Talebi, H.; Dimakis, A. G.; and Milanfar, P. 2022. Soft diffusion: Score matching for general corruptions. *arXiv preprint arXiv:2209.05442*.
- Feng, S.; Miao, C.; Zhang, Z.; and Zhao, P. 2024. Latent diffusion transformer for probabilistic time series forecasting. In *AAAI*, 11979–11987.
- Fons, E.; Sztrajman, A.; El-Laham, Y.; Ferrer, L.; Vyetrenko, S.; and Veloso, M. 2025. LSCD: Lomb-Scargle Conditioned Diffusion for Time series Imputation. *ICML*.
- Gao, J.; Cao, Q.; and Chen, Y. 2025. Auto-regressive moving diffusion models for time series forecasting. In *AAAI*, 16727–16735.
- Gong, D.; Liu, L.; Le, V.; Saha, B.; Mansour, M. R.; Venkatesh, S.; and Hengel, A. v. d. 2019. Memorizing normality to detect anomaly: Memory-augmented deep autoencoder for unsupervised anomaly detection. In *ICCV*, 1705–1714.
- Goswami, M.; Challu, C. I.; Callot, L.; Minorics, L.; and Kan, A. 2023. Unsupervised Model Selection for Time Series Anomaly Detection. In *ICLR*.
- Ho, J.; Jain, A.; and Abbeel, P. 2020. Denoising diffusion probabilistic models. *NeurIPS*, 33: 6840–6851.
- Huang, H.; Chen, M.; and Qiao, X. 2024. Generative Learning for Financial Time Series with Irregular and Scale-Invariant Patterns. In *ICLR*.
- Ismail Fawaz, H.; Forestier, G.; Weber, J.; Idoumghar, L.; and Muller, P.-A. 2019. Deep learning for time series classification: a review. *Data mining and knowledge discovery*, 33(4): 917–963.
- Kascenas, A.; Sanchez, P.; Schrempf, P.; Wang, C.; Clackett, W.; Mikhael, S. S.; Voisey, J. P.; Goatman, K.; Weir, A.; Pugeault, N.; et al. 2023. The role of noise in denoising models for anomaly detection in medical images. *Medical Image Analysis*, 90: 102963.
- Kim, S.; Choi, K.; Choi, H.-S.; Lee, B.; and Yoon, S. 2022. Towards a rigorous evaluation of time-series anomaly detection. In *AAAI*, volume 36, 7194–7201.
- Kollovich, M.; Ansari, A. F.; Bohlke-Schneider, M.; Zschiegner, J.; Wang, H.; and Wang, Y. B. 2024. Predict, refine, synthesize: Self-guiding diffusion models for probabilistic time series forecasting. *NeurIPS*, 36.
- Kong, Z.; Ping, W.; Huang, J.; Zhao, K.; and Catanzaro, B. 2021. DiffWave: A Versatile Diffusion Model for Audio Synthesis. In *ICLR*.
- Li, Y.; Chen, W.; Hu, X.; Chen, B.; Zhou, M.; et al. 2024. Transformer-Modulated Diffusion Models for Probabilistic Multivariate Time Series Forecasting. In *ICLR*.
- Li, Y.; Meng, H.; Bi, Z.; Urnes, I. T.; and Chen, H. 2025. Population Aware Diffusion for Time Series Generation. In *AAAI*, 18520–18529.
- Li, Z.; Zhao, Y.; Han, J.; Su, Y.; Jiao, R.; Wen, X.; and Pei, D. 2021. Multivariate time series anomaly detection and interpretation using hierarchical inter-metric and temporal embedding. In *KDD*, 3220–3230.
- Lin, L.; Li, Z.; Li, R.; Li, X.; and Gao, J. 2024. Diffusion models for time-series applications: a survey. *Frontiers of Information Technology & Electronic Engineering*, 25(1): 19–41.
- Liu, F. T.; Ting, K. M.; and Zhou, Z.-H. 2008. Isolation Forest. In *ICDM*, 413–422.

- Liu, Q.; and Paparrizos, J. 2024. The Elephant in the Room: Towards A Reliable Time-Series Anomaly Detection Benchmark. In *NeurIPS*.
- Malhotra, P.; Ramakrishnan, A.; Anand, G.; Vig, L.; Agarwal, P.; and Shroff, G. 2016. LSTM-based encoder-decoder for multi-sensor anomaly detection. *arXiv preprint arXiv:1607.00148*.
- Nachmani, E.; Roman, R. S.; and Wolf, L. 2021. Non gaussian denoising diffusion models. *arXiv preprint arXiv:2106.07582*.
- Nam, Y.; Yoon, S.; Shin, Y.; Bae, M.; Song, H.; Lee, J.-G.; and Lee, B. S. 2024. Breaking the Time-Frequency Granularity Discrepancy in Time-Series Anomaly Detection. In *WWW*, 4204–4215.
- Narasimhan, S. S.; Agarwal, S.; Akcin, O.; sujay sanghavi; and Chinchali, S. P. 2024. Time Weaver: A Conditional Time Series Generation Model. In *ICML*.
- Obata, K.; Matsubara, Y.; and Sakurai, Y. 2025. Robust and Explainable Detector of Time Series Anomaly via Augmenting Multiclass Pseudo-Anomalies. In *KDD*.
- Paparrizos, J.; Boniol, P.; Palpanas, T.; Tsay, R. S.; Elmore, A.; and Franklin, M. J. 2022. Volume under the surface: a new accuracy evaluation measure for time-series anomaly detection. *Proc. VLDB Endow.*, 15(11): 2774–2787.
- Park, D.; Hoshi, Y.; and Kemp, C. C. 2018. A multimodal anomaly detector for robot-assisted feeding using an lstm-based variational autoencoder. *IEEE Robotics and Automation Letters*, 3(3): 1544–1551.
- Park, D.; Kim, H.; Hoshi, Y.; Erickson, Z.; Kapusta, A.; and Kemp, C. C. 2017. A multimodal execution monitor with anomaly classification for robot-assisted feeding. In *2017 IEEE/RSJ International Conference on Intelligent Robots and Systems (IROS)*, 5406–5413. IEEE.
- Pintilie, I.; Manolache, A.; and Brad, F. 2023. Time series anomaly detection using diffusion-based models. In *2023 IEEE International Conference on Data Mining Workshops (ICDMW)*, 570–578. IEEE.
- Rasul, K.; Seward, C.; Schuster, I.; and Vollgraf, R. 2021. Autoregressive denoising diffusion models for multivariate probabilistic time series forecasting. In *ICML*, 8857–8868. PMLR.
- Ronneberger, O.; Fischer, P.; and Brox, T. 2015. U-net: Convolutional networks for biomedical image segmentation. In *Medical image computing and computer-assisted intervention—MICCAI 2015: 18th international conference, Munich, Germany, October 5-9, 2015, proceedings, part III 18*, 234–241. Springer.
- Sarfraz, M. S.; Chen, M.-Y.; Layer, L.; Peng, K.; and Koulakis, M. 2024. Position: Quo Vadis, Unsupervised Time Series Anomaly Detection? In *ICML*.
- Schmidl, S.; Wenig, P.; and Papenbrock, T. 2022. Anomaly Detection in Time Series: A Comprehensive Evaluation. *Proceedings of the VLDB Endowment (PVLDB)*, 15(9): 1779–1797.
- Schölkopf, B.; Williamson, R. C.; Smola, A.; Shawe-Taylor, J.; and Platt, J. 1999. Support vector method for novelty detection. *NeurIPS*, 12.
- Shentu, Q.; Li, B.; Zhao, K.; Shu, Y.; Rao, Z.; Pan, L.; Yang, B.; and Guo, C. 2025. Towards a General Time Series Anomaly Detector with Adaptive Bottlenecks and Dual Adversarial Decoders. In *ICLR*.
- Su, Y.; Zhao, Y.; Niu, C.; Liu, R.; Sun, W.; and Pei, D. 2019. Robust anomaly detection for multivariate time series through stochastic recurrent neural network. In *KDD*, 2828–2837.
- Tan, S. C.; Ting, K. M.; and Liu, T. F. 2011. Fast anomaly detection for streaming data. In *AAAI, IJCAI'11*, 1511–1516. AAAI Press. ISBN 9781577355144.
- Tashiro, Y.; Song, J.; Song, Y.; and Ermon, S. 2021. Csd: Conditional score-based diffusion models for probabilistic time series imputation. *NeurIPS*, 34: 24804–24816.
- Tatbul, N.; Lee, T. J.; Zdonik, S.; Alam, M.; and Gottschlich, J. 2018. Precision and recall for time series. In *NeurIPS, NIPS'18, 1924–1934*. Red Hook, NY, USA: Curran Associates Inc.
- Tishby, N.; and Zaslavsky, N. 2015. Deep learning and the information bottleneck principle. In *2015 IEEE information theory workshop (itw)*, 1–5. IEEE.
- Tuli, S.; Casale, G.; and Jennings, N. R. 2022. TranAD: Deep Transformer Networks for Anomaly Detection in Multivariate Time Series Data. *Proceedings of VLDB*, 15(6): 1201–1214.
- Vaswani, A.; Shazeer, N.; Parmar, N.; Uszkoreit, J.; Jones, L.; Gomez, A. N.; Kaiser, Ł.; and Polosukhin, I. 2017. Attention is all you need. *NeurIPS*, 30.
- Vincent, P.; Larochelle, H.; Lajoie, I.; Bengio, Y.; Manzagol, P.-A.; and Bottou, L. 2010. Stacked denoising autoencoders: Learning useful representations in a deep network with a local denoising criterion. *Journal of machine learning research*, 11(12).
- Wang, C.; Zhuang, Z.; Qi, Q.; Wang, J.; Wang, X.; Sun, H.; and Liao, J. 2024a. Drift doesn't matter: dynamic decomposition with diffusion reconstruction for unstable multivariate time series anomaly detection. *NeurIPS*, 36.
- Wang, C.; Zhuang, Z.; Qi, Q.; Wang, J.; Wang, X.; Sun, H.; and Liao, J. 2024b. Drift doesn't matter: dynamic decomposition with diffusion reconstruction for unstable multivariate time series anomaly detection. *NeurIPS*, 36.
- Wang, X.; Zhang, H.; Wang, P.; Zhang, Y.; Wang, B.; Zhou, Z.; and Wang, Y. 2023. An Observed Value Consistent Diffusion Model for Imputing Missing Values in Multivariate Time Series. In *KDD, KDD '23*, 2409–2418.
- Wu, R.; and Keogh, E. J. 2021. Current time series anomaly detection benchmarks are flawed and are creating the illusion of progress. *IEEE transactions on knowledge and data engineering*, 35(3): 2421–2429.
- Wu, S.; Zhao, J.; and Tian, G. 2022. Understanding and Mitigating Data Contamination in Deep Anomaly Detection: A Kernel-based Approach. In *IJCAI*, 2319–2325.
- Wyatt, J.; Leach, A.; Schmon, S. M.; and Willcocks, C. G. 2022. Anoddp: Anomaly detection with denoising diffusion probabilistic models using simplex noise. In *CVPR*, 650–656.

Xiao, C.; Gou, Z.; Tai, W.; Zhang, K.; and Zhou, F. 2023. Imputation-based time-series anomaly detection with conditional weight-incremental diffusion models. In *KDD*, 2742–2751.

Xu, H.; Chen, W.; Zhao, N.; Li, Z.; Bu, J.; Li, Z.; Liu, Y.; Zhao, Y.; Pei, D.; Feng, Y.; et al. 2018. Unsupervised anomaly detection via variational auto-encoder for seasonal kpis in web applications. In *WWW*, 187–196.

Xu, J.; Wu, H.; Wang, J.; and Long, M. 2022. Anomaly Transformer: Time Series Anomaly Detection with Association Discrepancy. In *ICLR*.

Yang, L.; Zhang, Z.; Song, Y.; Hong, S.; Xu, R.; Zhao, Y.; Zhang, W.; Cui, B.; and Yang, M.-H. 2023a. Diffusion Models: A Comprehensive Survey of Methods and Applications. *ACM Comput. Surv.*, 56(4).

Yang, Y.; Zhang, C.; Zhou, T.; Wen, Q.; and Sun, L. 2023b. Dcdetector: Dual attention contrastive representation learning for time series anomaly detection. In *KDD*, 3033–3045.

You, Z.; Cui, L.; Shen, Y.; Yang, K.; Lu, X.; Zheng, Y.; and Le, X. 2022. A unified model for multi-class anomaly detection. *NeurIPS*, 35: 4571–4584.

Yue, W.; Ying, X.; Guo, R.; Chen, D.; Shi, J.; Xing, B.; Zhu, Y.; and Chen, T. 2024. Sub-Adjacent Transformer: Improving Time Series Anomaly Detection with Reconstruction Error from Sub-Adjacent Neighborhoods. *arXiv preprint arXiv:2404.18948*.

Zhang, C.; Zhang, C.; Zhang, M.; and Kweon, I. S. 2023a. Text-to-image diffusion models in generative ai: A survey. *arXiv preprint arXiv:2303.07909*.

Zhang, S.; Wang, S.; Tan, X.; Liu, R.; Zhang, J.; and Wang, J. 2023b. sasdim: self-adaptive noise scaling diffusion model for spatial time series imputation. *arXiv preprint arXiv:2309.01988*.

Zhong, G.; Yuan, J.; Li, Z.; Chen, L.; et al. 2025. Multi-resolution decomposable diffusion model for non-stationary time series anomaly detection. In *ICLR*.

Zhou, B.; Liu, S.; Hooi, B.; Cheng, X.; and Ye, J. 2019. Beatgan: Anomalous rhythm detection using adversarially generated time series. In *IJCAI*, volume 2019, 4433–4439.

	UCR	AIOps	Yahoo real	Yahoo bench	SMD
# of Subdatasets	250	29	37	181	28
# of Features	1	1	1	1	38
Domain	Various	Cloud KPIs	Web traffic	Synthetic	Server
	<i>Train (Average per subdataset)</i>				
Sequence Length	30522	103588	860	1008	25300
# of Anomalies	0.00	42.35	0.84	5.53	-
Anomaly Ratio (%)	0.00	2.49	0.87	0.55	-
	<i>Test (Average per subdataset)</i>				
Sequence Length	56173	100649	573	672	25300
# of Anomalies	1.00	50.69	2.49	3.97	11.68
Anomaly Ratio (%)	0.85	1.81	4.58	0.59	4.21

Table 4: Statistics of the datasets.

Proof

Proposition 1 Assume we have a noise $\epsilon_t = \mathbf{B} \circ \epsilon^1 + (\mathbf{1} - \mathbf{B}) \circ \epsilon^2$, where ϵ^1 and ϵ^2 are sampled from some distributions, and \mathbf{B} is a mask with elements drawn from a Bernoulli distribution, $\mathbf{B}_{k,l} \sim \text{Bernoulli}(p)$. Then, the loss function Equation (6) can be separated into two parts by the mask.

Proof 1 Each element of the mask is independent. Hence,

$$\begin{aligned}
\mathcal{L} &= \mathbb{E}[\|\epsilon_t - \epsilon_\theta(\mathbf{X}_t, t)\|] & (13) \\
&= \mathbb{E}[\|\mathbf{B} \circ \epsilon_t - \mathbf{B} \circ \epsilon_\theta(\mathbf{X}_t, t)\|] \\
&\quad + \mathbb{E}[\|(\mathbf{1} - \mathbf{B}) \circ \epsilon_t - (\mathbf{1} - \mathbf{B}) \circ \epsilon_\theta(\mathbf{X}_t, t)\|] \\
&= \mathbb{E}[\|\mathbf{B} \circ \epsilon^1 - \mathbf{B} \circ \epsilon_\theta(\mathbf{X}_t, t)\|] \\
&\quad + \mathbb{E}[\|(\mathbf{1} - \mathbf{B}) \circ \epsilon^2 - (\mathbf{1} - \mathbf{B}) \circ \epsilon_\theta(\mathbf{X}_t, t)\|] \\
&= \mathbb{E}[\|\mathbf{B} \circ \epsilon^1 - \mathbf{B} \circ \epsilon_\theta(\mathbf{X}_t, t)\|] \\
&\quad + \mathbb{E}[\|(\mathbf{1} - \mathbf{B}) \circ \epsilon^2 - (\mathbf{1} - \mathbf{B}) \circ \epsilon_\theta(\mathbf{X}_t, t)\|] \\
&= \mathbb{E}[\|\mathbf{B} \circ \epsilon^1 - \epsilon_\theta(\mathbf{X}_t, t)\|] + \mathbb{E}[\|(\mathbf{1} - \mathbf{B}) \circ \epsilon^2 - \epsilon_\theta(\mathbf{X}_t, t)\|].
\end{aligned}$$

Our masked Gaussian noise is a special case of the above, where $\epsilon^1 = \zeta \sim \mathcal{N}(\mathbf{0}, \mathbf{I})$ and $\epsilon^2 = \mathbf{0}$ is deterministic.

Thus, we have

$$\begin{aligned}
\mathcal{L} &= \mathbb{E}[\|\epsilon_t - \epsilon_\theta(\mathbf{X}_t, t)\|] & (14) \\
&= \underbrace{\mathbb{E}[\|\mathbf{B} \circ \zeta - \epsilon_\theta(\mathbf{X}_t, t)\|]}_{\text{Noisy part}} + \underbrace{\mathbb{E}[\|(\mathbf{1} - \mathbf{B}) \circ \mathbf{0} - \epsilon_\theta(\mathbf{X}_t, t)\|]}_{\text{Noiseless part}} \\
&= \mathcal{L}_{NonMask} + \mathcal{L}_{Mask}.
\end{aligned}$$

Experiment Setup

Datasets

We provide a detailed description of the datasets and their statistics (Table 4).

- UCR anomaly archive (UCR) (Wu and Keogh 2021): contains 250 diverse univariate time series from various domains. According to (Goswami et al. 2023), the datasets include nine domains, (1) Acceleration, (2) Air Temperature, (3) Arterial Blood Pressure (ABP), (4) Electrical Penetration Graph (EPG), (5) Electrocardiogram (ECG), (6) Gait, (7) NASA, (8) Power Demand, and (9) Respiration (RESP). There is only one well-checked anomaly in each sequence, which overcomes some of the flaws in previously used benchmarks.

- AIOps¹: comprises 29 univariate time series of Key Performance Indicators (KPIs), which are monitored to provide a stable web service from prominent Internet companies.
- Yahoo real and bench²: are provided as part of the Yahoo! Webscope program. Yahoo real contains real production traffic to some of the Yahoo! properties, and Yahoo bench contains synthetic time series, including components such as trend and seasonality.
- Server Machine Dataset (SMD) (Su et al. 2019): comprises a multivariate time series with 38 features from 28 server machines collected from a large internet company over a period of five weeks. Both the training and test sets contain around 50k timestamps with 5% anomalous cases. Although the use of SMD has generated both support (Challu et al. 2022; Goswami et al. 2023) and opposition (Wu and Keogh 2021), we employ this dataset because of its multivariate nature.

Baselines

We detail the baselines below.

- IsolationForest (Liu, Ting, and Zhou 2008): constructs binary trees based on random space splitting. The nodes with shorter path lengths to the root are more likely to be anomalies.
- OCSVM (Schölkopf et al. 1999): uses the smallest possible hypersphere to encompass instances. The distance from the hypersphere to data located outside the hypersphere is used to determine whether or not the data are anomalous.
- BeatGAN (Zhou et al. 2019): is based on a GAN framework where reconstructions produced by the generator are regularized by the discriminator instead of fixed reconstruction loss functions.
- LSTM-VAE (Park, Hoshi, and Kemp 2018): is an LSTM-based VAE capturing complex temporal dependencies that models the data-generating process from the latent space to the observed space, which is trained using variational techniques.
- USAD (Audibert et al. 2020): presents an autoencoder architecture whose adversarial-style learning is also inspired by GAN.
- Anomaly-Transformer (Xu et al. 2022): combines series and prior association to make anomalies distinctive.
- TranAD (Tuli, Casale, and Jennings 2022): is a Transformer-based model that uses attention-based sequence encoders to perform inferences with broader temporal trends, focusing on score-based self-conditioning for robust multi-modal feature extraction and adversarial training.
- DADA (Shentu et al. 2025): is a zero-shot anomaly detector designed for multi-domain time series. It features

¹<https://competition.aiops-challenge.com/home/competition/1484452272200032281>

²<https://webscope.sandbox.yahoo.com/catalog.php?datatype=s&did=70>

Design Parameter	Value
<i>Architecture</i>	
Attention heads	8
# of residual blocks N	8
Latent dimension C	64
<i>Diffusion model</i>	
Forward diffusion step T	50
Reverse diffusion step λ	50
Noise scheduling β	$\text{np.linspace}(\beta_{start}, \beta_{end}, T)$
Minimum noise β_{start}	0.0001
Maximum noise β_{end}	0.01
Bernoulli parameter p	0.5

Table 5: Key hyperparameters for AnomalyFilter.

Adaptive Bottlenecks for flexible latent space compression based on data characteristics, and Dual Adversarial Decoders that explicitly distinguish normal from anomalous patterns through adversarial training.

- DiffAD (Xiao et al. 2023): is a conditional diffusion model that employs a density ratio-based strategy as a conditioner. Its conditioner is based on density-based selection, where only the high-density (i.e., normal) parts of the sample are provided to the model.
- IMDiffusion (Chen et al. 2023): integrates the imputation method with a grating masking strategy and conditional diffusion model. It masks half of a sequence and uses the unmasked portion as the conditioner to reconstruct the masked part. Then, it reverses the mask and reconstructs the entire sequence. The reconstruction is gradually generated from white noise through the denoising process.
- D3R (Wang et al. 2024b): is a denoising model that tackles the drift via decomposition and reconstruction, overcoming the limitation of the local sliding window. It first extracts stable components by decomposition. Then, it disturbs the stable components by adding noise and learns denoising. The reconstruction is conducted at 1 step, similar to DAE.
- DAE (Vincent et al. 2010): corrupts the sample with $\hat{\mathbf{X}} = \mathbf{X} + \alpha\epsilon$, where we use $\alpha = 0.1, \epsilon \sim \mathcal{N}(\mathbf{0}, \mathbf{I})$, and directly predicts the clean sample \mathbf{X} . We use the same hyperparameters and model architecture with AnomalyFilter.
- DDPM (Ho, Jain, and Abbeel 2020): trains the model by Algorithm 1 and reconstructs learned samples from corrupted data by Algorithm 2. We use the same hyperparameters and model architecture with AnomalyFilter.

To ensure a fair comparison of reconstruction quality, all reconstruction-based methods used in this study employed MSE as the anomaly score. To handle sequential information, we then apply the moving average of half of the window size (50 timesteps) to the score.

Implementation Details

We train the proposed model using AdamW with a learning rate of 10^{-3} . The batch size is 64. We use 10% of the

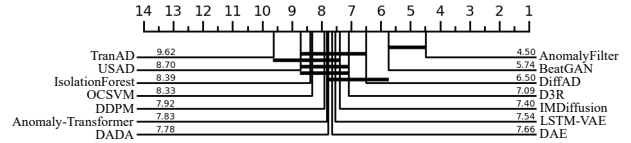


Figure 4: Critical difference diagram of VUS-PR.

training samples as validation and apply early stopping for a maximum of 100 epochs. Other hyperparameters related to the framework are listed in Table 5. Due to the out-of-memory issue, we used $N = 4, C = 32$ for SMD. The baselines are implemented based on previously reported hyperparameters and are trained with early stopping using a procedure similar to AnomalyFilter. The window size is 100 for all datasets.

Experimental Results

Results of Various Metrics

We show the corresponding results of other range-based metrics, Range-AUC-ROC and Range-AUC-PR, in Table 6, as well as standard deviation in Table 7. Figure 4 shows the corresponding critical difference diagram of VUS-PR based on the Wilcoxon-Holm method (Ismail Fawaz et al. 2019), where methods that are not connected by a bold line are significantly different in average rank. Overall, we observe that AnomalyFilter outperforms the baselines for most datasets and metrics.

Ablation Studies

Qualitative analysis We visualize the reconstruction when adding each component to DDPM. Figure 5 show the results of DDPM with each component and AnomalyFilter of #029 ABP data from UCR. The area where it appears that the noise is added to the normal peak is the anomaly, indicated with a red background. DDPM and DDPM w/ Mask struggle to accurately reconstruct the normal parts, leading to poor anomaly detection performance. DDPM w/ Noiseless improves reconstruction of the normal parts compared with DDPM, but still exhibits significant deviations in certain areas. In contrast, AnomalyFilter achieves notably low MSE for the normal parts, making anomalies stand out and enabling much more effective detection.

Sensitivity Analysis

We study the effect of key hyperparameters. Figure 6 shows VUS-ROC and VUS-PR of the average of all datasets.

Effect of ratio between noise and mask We investigate the effect of the Bernoulli mask by training models with masked Gaussian noise using different noise ratios p . Figure 6 (a) shows the results for both noiseless inference and naive inference. When $p = 0.0$, Gaussian noise is not added at all, and the model learns to scale the data based on the noise schedule, resulting in low accuracy with both inference procedures. $p = 1.0$ indicates the addition of Gaussian noise. For noiseless inference, the best performance was

	UCR				AIOps				Yahoo real				Yahoo bench				SMD			
	R-R	R-P	A-R	F																
IsolationForest	0.653	0.114	0.613	0.057	0.825	0.217	0.824	0.187	0.813	0.595	0.601	0.000	0.705	0.487	0.502	0.000	0.764	0.275	0.799	0.171
OCSVM	0.662	0.187	0.618	0.092	0.874	0.463	0.866	0.220	0.841	0.722	0.633	0.000	0.710	0.516	0.523	0.000	0.727	0.274	0.801	0.254
BeatGAN	0.752	0.209	0.729	0.158	0.912	0.594	0.814	0.214	0.852	0.723	0.655	0.063	0.799	0.577	0.624	0.005	0.829	0.383	0.857	0.325
LSTM-VAE	0.745	0.140	0.719	0.117	0.881	0.419	0.830	0.197	0.934	0.782	0.846	0.092	0.781	0.520	0.617	0.003	0.732	0.239	0.798	0.266
USAD	0.684	0.157	0.651	0.138	0.908	0.541	0.862	0.221	0.892	0.758	0.771	0.081	0.695	0.485	0.527	0.000	0.550	0.183	0.583	0.118
Anomaly-Transformer	0.720	0.138	0.675	0.106	0.901	0.442	0.847	0.146	0.915	0.749	0.799	0.069	0.790	0.487	0.604	0.005	0.874	0.457	0.885	0.342
TranAD	0.609	0.072	0.537	0.059	0.789	0.273	0.798	0.261	0.844	0.666	0.712	0.068	0.678	0.449	0.502	0.000	0.693	0.259	0.604	0.159
DADA	0.610	0.031	0.542	0.016	0.863	0.306	0.764	0.156	0.911	0.727	0.768	0.113	0.822	0.508	0.624	0.006	0.885	0.445	0.867	0.326
DiffAD	0.623	0.065	0.578	0.044	0.893	0.500	0.783	0.192	0.899	0.725	0.760	0.088	0.838	0.560	0.670	0.004	0.644	0.188	0.681	0.199
IMDiffusion	0.651	0.050	0.596	0.032	0.889	0.435	0.795	0.116	0.907	0.751	0.782	0.075	0.799	0.489	0.605	0.001	0.865	0.367	0.867	0.229
D3R	0.610	0.074	0.534	0.061	0.871	0.492	0.804	0.199	0.902	0.767	0.764	0.109	0.765	0.507	0.543	0.000	0.846	0.368	0.833	0.321
AnomalyFilter	0.740	0.245	0.697	0.196	0.943	0.690	0.854	0.227	0.933	0.813	0.833	0.128	0.852	0.621	0.686	0.013	0.900	0.508	0.873	0.321

Table 6: R-R, R-P, A-R, and F are Range-AUC-ROC, Range-AUC-PR (Paparrizos et al. 2022), AUC-ROC, and F1.

	UCR				AIOps			Yahoo real			Yahoo bench			SMD		
	V-R	V-P	RF	Acc.	V-R	V-P	RF	V-R	V-P	RF	V-R	V-P	RF	V-R	V-P	RF
IsolationForest	0.262	0.201	0.125	0.425	0.103	0.125	0.077	0.220	0.193	0.000	0.195	0.176	0.000	0.145	0.189	0.104
OCSVM	0.271	0.267	0.203	0.459	0.115	0.201	0.132	0.225	0.218	0.000	0.210	0.173	0.000	0.159	0.202	0.199
BeatGAN	0.232	0.280	0.206	0.478	0.116	0.222	0.129	0.217	0.224	0.114	0.186	0.229	0.019	0.144	0.226	0.189
LSTM-VAE	0.208	0.231	0.186	0.412	0.117	0.207	0.125	0.125	0.269	0.161	0.195	0.223	0.021	0.147	0.181	0.210
USAD	0.235	0.257	0.233	0.446	0.123	0.235	0.145	0.196	0.267	0.148	0.235	0.214	0.000	0.201	0.135	0.123
Anomaly-Transformer	0.227	0.239	0.198	0.401	0.101	0.166	0.096	0.149	0.246	0.097	0.159	0.191	0.026	0.122	0.217	0.216
TranAD	0.215	0.165	0.177	0.364	0.149	0.177	0.136	0.219	0.272	0.139	0.221	0.183	0.008	0.228	0.172	0.123
DADA	0.200	0.065	0.053	0.187	0.117	0.179	0.090	0.173	0.295	0.192	0.151	0.195	0.028	0.113	0.199	0.174
DiffAD	0.244	0.155	0.111	0.294	0.134	0.196	0.130	0.174	0.272	0.169	0.139	0.204	0.027	0.168	0.139	0.139
IMDiffusion	0.203	0.121	0.089	0.238	0.128	0.202	0.144	0.172	0.256	0.143	0.162	0.198	0.014	0.122	0.215	0.211
D3R	0.219	0.162	0.171	0.364	0.157	0.237	0.137	0.169	0.238	0.163	0.202	0.186	0.006	0.110	0.214	0.197
AnomalyFilter	0.234	0.308	0.267	0.490	0.098	0.166	0.100	0.143	0.237	0.179	0.162	0.229	0.029	0.112	0.227	0.194

Table 7: Standard deviation of VUS-ROC, VUS-PR, and Range F-score.

achieved at $p = 0.5$, demonstrating that effective learning of the filter requires balancing both the denoise and retain functionalities. On the other hand, for naive inference, $p = 1.0$ yielded the best performance, indicating that reconstruction from corrupted data requires the model to be trained with noise that aligns closely with the inference conditions.

Effect of noise schedule We use a linear variance schedule to define the noise schedule. β_{end} determines the maximum noise level, and we vary it across $\{0.001, 0.005, 0.01, 0.05, 0.1\}$. The results in Figure 6 (b) indicate that an optimal level of noise is necessary for the best performance.

Effect of forward diffusion step We vary the forward diffusion step T across $\{1, 2, 4, 8, 16, 32, 50\}$, with the reverse diffusion step λ set at the same value as T . Shorter steps lead to more rapid corruption. When $T = 1$, the model denoises in a single step, resembling DAE and achieving similar accuracy. The results in Figure 6 (c) indicate that a $T \geq 32$ is sufficient for effective performance. Shorter steps are preferable when using naive inference, suggesting that the denoising step should ideally operate in a noise-free setting.

Effect of reverse diffusion step We fix the forward diffusion step $T = 50$ and vary the reverse diffusion step λ across $\{1, 2, 4, 8, 16, 32, 50\}$. As shown in Figure 6 (d) $\lambda \geq 8$ is sufficient for effective performance. With naive inference, the best accuracy is achieved at $\lambda = 8$, indicating that using a relatively small λ compared with T improves performance. However, the results also show that an overly short λ compared with T hinders effective denoising, which requires careful tuning of λ .

Computational Time

We select six denoising-based methods to evaluate their scalability with respect to varying sample sizes during training and inference. For diffusion models, we set forward and reverse diffusion steps to 50. All methods are evaluated under the same NVIDIA RTX A6000. As shown in Figure 7 (a), the training times are comparable across methods, except for D3R. During inference shown in Figure 7 (b), DAE and D3R, which predict in a single step, are faster than the others. Diffusion-based methods that require multiple reverse diffusion steps exhibit similar inference times.

Case Studies

We present further case studies in Figure 8 that visually show the difference between baselines and AnomalyFilter.

AIOps KPI-301c This dataset consists of noisy sequences whose values fluctuate in a fine-grained manner, as shown in Figure 8 (a). It includes different types of anomalies, such as a pattern anomaly at around timestep 1600 and many point anomalies. AnomalyFilter has a higher reconstruction error for all anomalies visualized in the figure, while accurately reconstructing normal parts. In contrast, other methods fail to detect anomalies because their reconstruction error on normal parts is relatively larger than that of anomalous parts.

Yahoo real A1real-28 The Yahoo dataset provides limited training data, and some test data exhibit characteristics different from the training data. As shown in Figure 8 (b), this sequence contains a cutoff anomaly shortly after the start of the test period (around timestep 1000), as well as two point anomalies. Due to the limited amount of training data, all

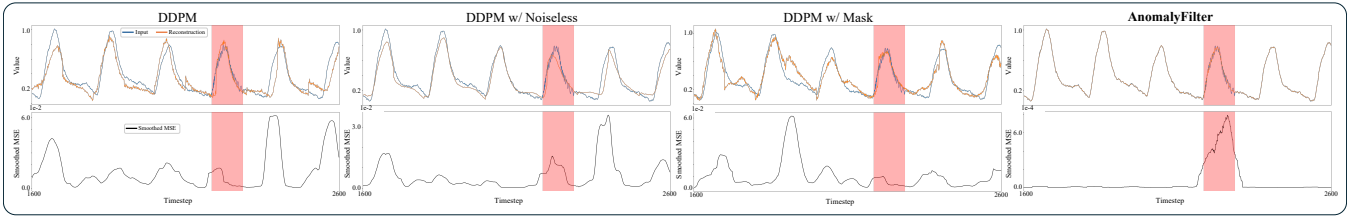


Figure 5: Reconstruction examples across DDPM variants of #029 ABP on UCR.

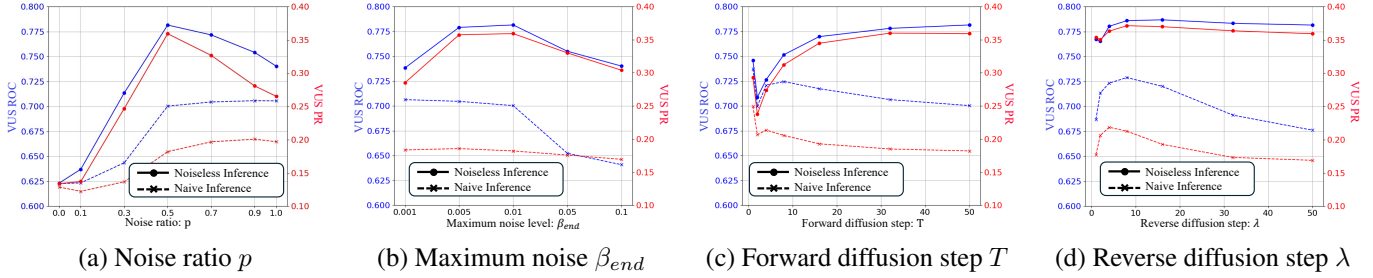


Figure 6: Sensitivity analysis across four hyperparameters.

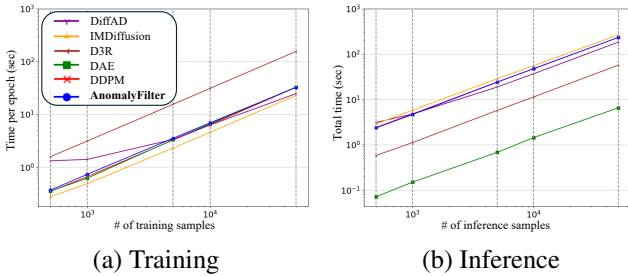


Figure 7: Computational time for training and inference.

methods struggle to detect the cutoff anomaly. Only AnomalyFilter has a high reconstruction error for the subsequent point anomalies.

Yahoo bench A3Benchmark-TS3 Figure 8 (c) is from Yahoo bench. This dataset includes a trend component, causing the test values to fall outside the range of the training data. BeatGAN fails to shift the baseline of the reconstruction, resulting in a gradual drift away from the input. Although Anomaly-Transformer and IMDiffusion handle the baseline shift of test data, their large reconstruction error leads to failures in anomaly detection. In contrast, AnomalyFilter, due to its gradual denoising nature from the input, produces a reconstruction that closely matches the input and successfully detects the point anomalies.

SMD machine-1-6 We show the results of SMD on Figure 8 (d). In the SMD dataset, each variable in the multivariate time series is individually labeled for anomalies; however, as visualized, the labeling accuracy is often low. Therefore, we adopt a commonly used setting where a time point is considered anomalous if any variable exhibits an anomaly. Because both BeatGAN and Anomaly-Transformer recon-

struct from the latent space, the reconstruction errors for dim3 and dim4 increase after timestep 4000, causing earlier anomalies to become less distinguishable. Moreover, the reconstruction of dim2 for BeatGAN and dim1 for Anomaly-Transformer is affected by dim3 and dim4, as these methods reconstruct the whole dimensions from the common latent vector. In contrast, denoising-based methods, which denoise from the input, maintain low reconstruction errors for dim3 and dim4, thereby avoiding such drifts. Since AnomalyFilter selectively denoises only the anomalous parts, it is less susceptible to the influence of anomalies in other variables.

More Related Work

Reconstruction-based Method for TSAD Inspired by the success of deep learning, numerous deep learning methods for TSAD have been proposed, with reconstruction-based methods constituting a significant proportion (Schmidl, Wenig, and Papenbrock 2022). Reconstruction-based methods aim to detect anomalous behavior in an unsupervised manner by comparing the original input with the reconstruction. They rely on the hypothesis that a model trained mostly on normal samples excels in normal parts but struggles in anomalous parts. Deep generative techniques, including VAE (Xu et al. 2018; Li et al. 2021) and GAN (Bashar and Nayak 2020), are often utilized to build reconstruction-based methods. For example, LSTM was incorporated into VAE to learn temporal features (Park, Hoshi, and Kemp 2018; Su et al. 2019). BeatGAN (Zhou et al. 2019), proposed for detecting anomalies in ECG beats, is a GAN-based method that uses time series warping for data augmentation. However, VAE and GAN are usually difficult to train because they require a careful balance between the two networks. Transformer architecture (Nam et al. 2024; Xu et al. 2022; Yang et al. 2023b; Yue et al. 2024) has also been explored. TranAD (Tuli, Casale,

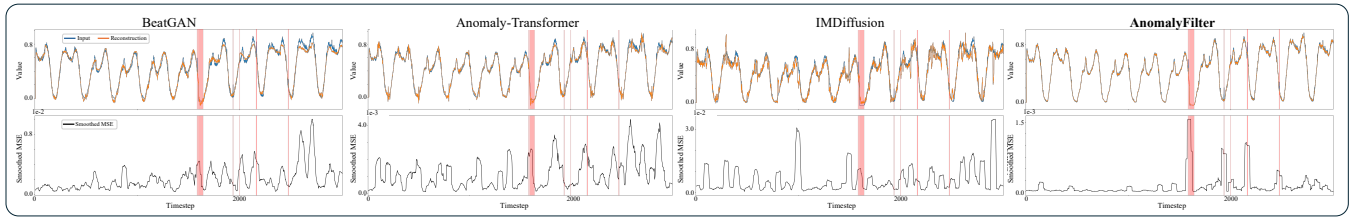
and Jennings 2022) introduces attention mechanisms from transformer models and incorporates adversarial training to jointly enhance the accuracy of anomaly detection. These encoder-decoder models aim to learn the latent representation for the entire time series for data reconstruction and can be interpreted through the information bottleneck (IB) principle, namely the trade-off between concise representation and reconstruction accuracy (Tishby and Zaslavsky 2015). However, in anomaly detection, controlling the IB is challenging due to the absence of anomaly knowledge and labels, often leading to underfitting (i.e., prioritizing conciseness) or overfitting (i.e., prioritizing reconstruction).

Limitations and Future Directions

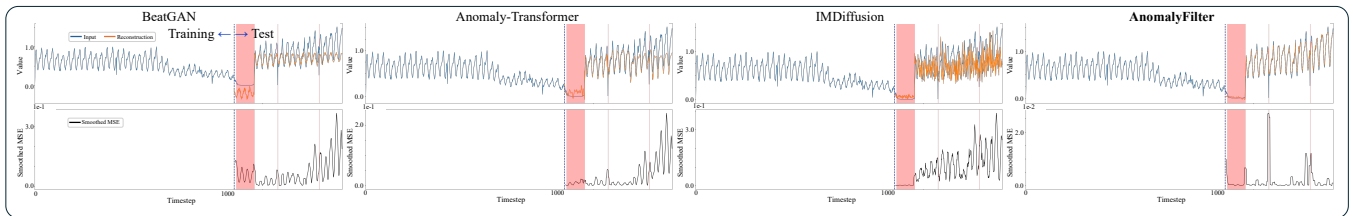
High-dimensional data Current benchmarks commonly used for multivariate time series anomaly detection assign the same label to all variables. While SMD labels individual variables, their quality is low, as we observed clearly normal variables labeled as anomalies. Therefore, models must predict anomalies if any variable in the multivariate data exhibits abnormal behavior.

Such labels mean that high-dimensional data pose challenges for AnomalyFilter, as the model learns noise that is independent across variables. This leads to reconstructions where only the anomalous parts of the affected variables are denoised. With MSE used as the anomaly score, the accumulation of errors across variables makes detecting anomalies increasingly difficult as the number of variables grows. On the other hand, when using encoder-decoder models, an anomaly in one variable affects the entire latent state, thereby influencing the reconstruction of all variables. Although they cannot pinpoint the specific anomalous variable, they are more suitable for the current labels. Accordingly, future research could focus on developing noise mechanisms that account for inter-variable dependencies.

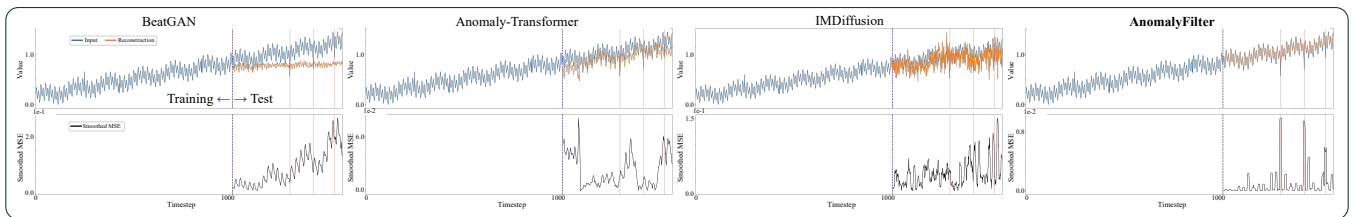
Anomaly contamination In unsupervised anomaly detection, it is common to assume that all or most of the training samples are normal, which is known as the normality assumption (Wu, Zhao, and Tian 2022). However, in real-world scenarios, the presence of anomaly samples in the training set (i.e., anomaly contamination) is inevitable (Obata, Matsubara, and Sakurai 2025). Under this assumption, reconstruction-based methods become vulnerable to contamination, as their strong representational power can lead to the accurate reconstruction of even anomalous patterns, thereby reducing performance. As with most of the reconstruction-based methods, we adopt the normality assumption, making AnomalyFilter susceptible to this issue. To the best of our knowledge, no diffusion-based approach has explicitly addressed anomaly contamination. Handling anomaly contamination within a diffusion-based framework remains an open and promising research direction.



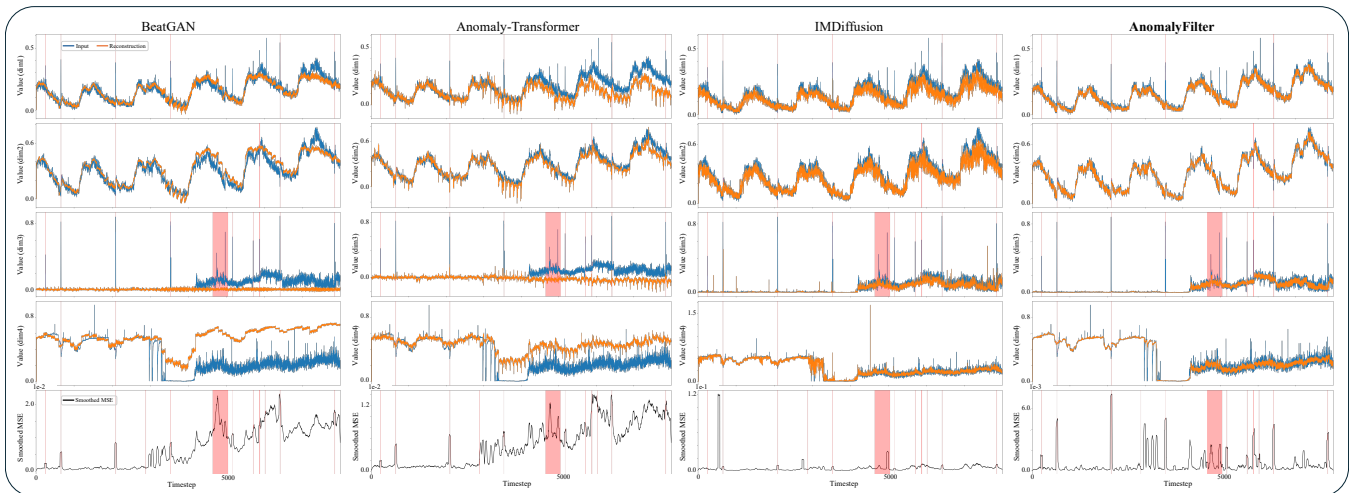
(a) AIOps KPI-301c



(b) Yahoo real A1real-28



(c) Yahoo bench A3Benchmark-TS3



(d) SMD machine-1-6

Figure 8: Reconstruction examples across different methods of (a) AIOps, (b) Yahoo real, (c) Yahoo bench, and (d) SMD.